Diffuse reflectance spectroscopy for determination of optical properties and chromophore concentrations of mice internal organs in the range of 350 nm to 1860 nm

Conference Paper · May 2018

DOI: 10.1117/12.2306636

7 authors, including:

Marcelo Saito Nogueira
Tyndall National Institute/University College Cork
58 PUBLICATIONS **437** CITATIONS

SEE PROFILE

Katarzyna Komolibus
Tyndall National Institute
18 PUBLICATIONS **59** CITATIONS

SEE PROFILE

Stefan andersson-engels
Tyndall National Institute
415 PUBLICATIONS **10,199** CITATIONS

SEE PROFILE

Diffuse reflectance spectroscopy for determination of optical properties and chromophore concentrations of mice internal organs in the range of 350 nm to 1860 nm

Marcelo Saito Nogueira[1,2], Michael Raju[1,2], Jacqueline Gunther[1], Konstantin Grygoryev[1], Katarzyna Komolibus[1], , Huihui Lu[1], and Stefan Andersson-Engels[1,2]
[1]Tyndall National Institute, Lee Maltings, Dyke Parade, Cork, Ireland
[2]Department of Physics, University College Cork, College Road, Cork, Ireland

ABSTRACT

The development of photomedical modalities for diagnostics and treatment has created a need for knowledge of the optical properties of the targeted biological tissues. These properties are essential to plan certain procedures, since they determine the light absorption, propagation and penetration in tissues. One way to measure these properties is based on diffuse reflectance spectroscopy (DRS). DRS can provide light absorption and scattering coefficients for each wavelength through a non-invasive, fast and *in situ* interrogation, and thereby tissue biochemical information. In this study, reflectance measurements of *ex vivo* mice organs were investigated in a wavelength range between 350 and 1860 nm. To the best of our knowledge, this range is broader than previous studies reported in the literature and is useful to study additional chromophores with absorption in the extended wavelength range. Also, it may provide a more accurate concentration of tissue chromophores when fitting the reflectance spectrum in this extended range. In order to extract these concentrations, optical properties were calculated in a wide spectral range through a fitting routine based on an inverse Monte-Carlo look-up table model. Measurements variability was assessed by calculating the Pearson correlation coefficients between each pair of measured spectra of the same type of organ.

Keywords: Optical properties, diffuse reflectance, optical spectroscopy, reflectance spectroscopy, optical diagnostics.

1. INTRODUCTION

Recent advancements in medical devices are progressing towards cost effective technologies capable of providing real-time and non-invasive assessment of biological tissues. Some of the technologies under development involve optical methods to enable functional imaging and customized therapy. Improvement of these methods is subject to the accuracy of the optical techniques employed. This creates a need for accurate determination of tissue optical properties of the tissues involved. For the purpose of diagnostics and therapy guidance, these properties can yield information of the tissue biochemistry. This will allow medical assessment at an earlier stage compared to current medical imaging technologies, which provide primarily morphological/structural information. Advancements rely on the ability to separate morphological and pathomorphological features (associated to scattering) from physiological properties of the tissue biochemistry (related to tissue absorption) in the captured optical signal. By detailing these two contributions, precise clinical interventions can be performed. These interventions are divided into optical diagnostics and treatment modalities. Therapeutic applications include precise laser surgery for quicker patient recovery, low level laser therapy for inflammation reduction and pain relief, laser-induced thermotherapy, and photodynamic therapy for a wide range of medical disorders [1-22]. On the other hand, applications in diagnostics include disease identification, monitoring diseases or healing progression, surgical guidance, and improvement of the effectiveness of treatment planning [23-31]. The efficiency of both optical diagnostics and treatments depends on tissue optical properties. These properties define light propagation inside biological tissues and can be used to apply correction factors to compensate the attenuation of the collected signal during tissue assessment [32-79] or to determine the light dose delivered during treatment customization [1-22]. In order to elucidate these properties, numerous research groups have developed techniques based on steady-state or time-resolved reflectance and transmittance measurements [13, 17, 80-88].

One of the main techniques for determination of optical properties is the diffuse reflectance spectroscopy (DRS) [89]. DRS is a promising cost effective tool for non-invasive, fast and *in situ* interrogation of biological tissues. It has

been employed in many clinical applications and is useful for tissue identification or evaluation of its composition [23-30]. In order to analyse DRS measurements, two approaches can be adopted. The first is tissue classification based on multivariate analysis [90-101]. Multivariate techniques are frequently employed to find discrimination between various tissue types, and where the optical *per se* are necessary. If the optical properties are to be derived, one often relies on the model based algorithms for data analysis. Then it is possible to extract the tissue optical properties, such as the absorption and reduced scattering coefficients [23-27, 29, 31, 89], as well as the chromophore concentrations [23-30]. To obtain the chromophore concentrations one employs the chromophore absorption spectrum, and a model for light propagation in tissue as inputs to a fitting algorithm. The light propagation model is either analytical (typically solving the radiative transport equation with the diffusion approximation) [102-115] or probabilistic (typically solving the radiative transport equation with Monte Carlo simulations) [27, 30, 88, 116-137].

Current analytical models are based on semi-empirical solutions or diffusion approximation, while look-up table (LUT) models are associated to an experimental reflectance database of measurements in tissue-mimicking phantoms or to a Monte Carlo (MC) database generated from forward MC simulations [27, 30, 133-137]. Inverse MC LUT models have the advantage of not depending on methodological differences of experimental measurements. Since these differences may hinder the comparison across reported studies [89], a standard reflectance database is key to guarantee the reproducibility of obtained results. Reproducibility is also dependent on the analysed wavelength range and on variations in ambient conditions during measurements [138-154]. With this in mind, these variations should be investigated in the widest wavelength range possible, including the scarcely studied near-infrared region above 1100 nm. In addition, further research is required to understand effects of pressure and temperature in reflectance measurements in order to apply a correction in the collected spectra.

In this study, we provide a preliminary analysis of the effect of pressure and temperature variations in diffuse reflectance spectra and total hemoglobin concentrations. Diffuse reflectance spectra were analysed in an extended wavelength range between 350 nm and 1860 nm. Chromophore concentrations were obtained by using an inverse MC LUT model to fit the reflectance spectrum. Our LUT covers a wider range of optical properties (scattering coefficient varying from 5 to 1500 cm^{-1} and absorption coefficient from 0.03 to 1000 cm^{-1}) and a greater resolution (676 reflectance values) than previously reported studies, to the best of our knowledge.

2. METHODOLOGY

2.1 Diffuse reflectance spectroscopy (DRS) system

This system has a broadband light source (HL-2000, Ocean Optics, Edinburgh, United Kingdom) that delivers the light to the sample through a 600-µm-core Low-OH-Silica fibre optic probe (BF46LS01 1-to-4 Fan-Out Bundle, Thorlabs, Munich, Germany) with 630 µm source-to-detector (fibre center-to-center) distance. By using the same probe, the reflected light is collected and sent to two detectors: one visible wavelength spectrometer (QE-Pro, Ocean Optics, Edinburgh, United Kingdom) and one near-infrared wavelength spectrometer (NIR-Quest, Ocean Optics, Edinburgh, United Kingdom). The intensity is measured for wavelengths in the range of 350 nm to 1860 nm (figure 1). After measuring the intensity, the data can be post-processed.

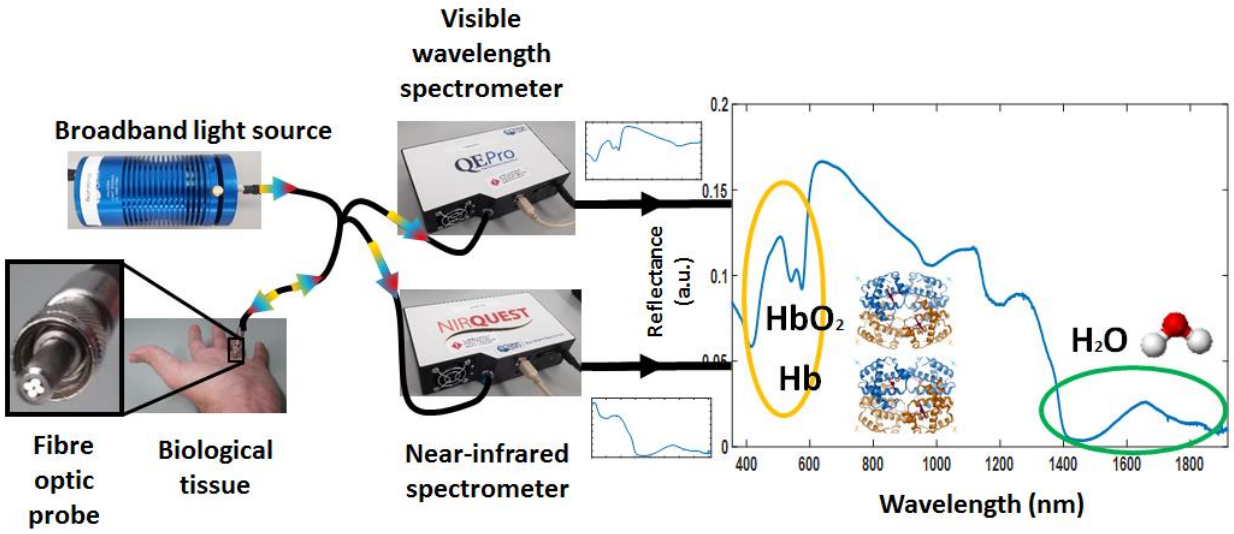

Figure 1: Schematic image of the DRS system. Reflected light can be collected in a wide range of wavelengths and, thus, allow the investigation of a larger variety of chromophores in biological tissues such as oxyhaemoglobin, deoxyhaemoglobin, and water. Our fibre probe has 600-µm-core fibres next to each other and a 630 µm source-to-detector (fibre center-to-center) distance is kept between them so that we collect a intense signal from scattered light.

2.2 Removal and preservation of mice internal organs

C57 mice were anesthetized and had their organs removed. This removal was performed after access to internal organs through 5 steps: initial incision below the navel going up toward the mouth, downward incision toward the tail, lateral incision at the shoulder joints, another at the pelvic girdle and removal of the abdominal membrane. Mice internal organs were taken away and washed with phosphate buffer saline solution to maintain physiological conditions. After this, they were preserved in a plastic container with phosphate buffer saline solution surrounded by ice until the start of the measurements.

Measurements were performed in two different temperatures (0 °C and 25 °C) and two pressure states (touching the surface of the fibre optic probe in the *ex vivo* tissue or gently pressing it). The gentle pressure simulates variations in reflectance due to attempts in keeping the probe in a stable position during measurements. In all different conditions, organs (2 hearts, 3 kidneys, and 3 livers) were covered with a plastic foil while immersed in phosphate buffer saline solution in order to avoid dehydration.

2.3 Data processing

Both visible and near-infrared spectra have their background subtracted and the captured signal is then divided by the results from a reflectance standard (FWS-99-01c, Avian Technologies LLC, New London, USA). Then, the visible and near-infrared spectra are connected in order to analyse chromophores concentration in a continuous broad spectrum. In order to ensure there were no variations due to system fluctuations, both background and reference signals were collected before and after our measurements.

2.4 Data analysis

Our spectral analysis consists in two approaches: reproducibility analysis and extraction of tissue optical properties. The former was based on the variability of the shape of the measured spectra. This was evaluated by calculating the Pearson correlation coefficient for each pair of measurements. On the other hand, determination of tissue optical

properties was performed by fitting each spectrum using an inverse MC LUT model. The outputs of this model are the scattering associated coefficients and biomolecules concentrations.

Measurements reproducibility was calculated by evaluating variations in the Pearson correlation coefficient among measurements in the same organ (internal reproducibility), among measurements in different organs (external reproducibility), and among measurement averages in the same organ (external average reproducibility). For the calculation of these coefficients, each pair of measurements was compared separately and the average of the coefficients was taken. In addition, organ biological variability was calculated by comparing the external and internal reproducibility using equation 1:

$$\text{Organ variability} = \frac{|External\ correlation\ average - Internal\ correlation\ average|}{Standard\ deviation\ of\ internal\ correlation} \quad (1)$$

Tissue optical properties including μ_a and μ_s are used as an input to a forward Monte Carlo model, which is used to simulate the light transport inside tissue and calculate the photon flux coming out of it in different positions. By calculating the photon flux in the area of our collection/detection fibre for each combination of absorption coefficient (μ_a) and scattering coefficient (μ_s) in a wide range of optical properties, we generated a look-up table (LUT) for the spectral fitting. The contribution of photons launched in the light source area, i.e., the area of our excitation fibre, is taken into account by performing a convolution for the incident photon beam. The resulting LUT is accessed by the fitting algorithm to find the best combination of chromophore concentrations and scattering parameters to best match the measured reflectance spectrum.

The spectral fitting is based on comparing the experimental spectra with the simulated photon reflectance coming out from biological tissue with specific optical properties [26]. We assumed a fixed anisotropy factor (g = 0.9). The variable parameters are total μ_a and μ_s, which must be a combination of biomolecules absorption in the wavelength range of the measurement and a combination of Mie and Rayleigh scattering, respectively (equation 2 and 3). The known spectral relations of the absorption spectra and scattering mechanisms relates the measurements at all wavelengths in the measured spectrum.

By using the generated LUT (reflectance database from forward Monte Carlo model), the spectral relations for Mie and Rayleigh scattering, and the absorption spectra from chromophores reported in the literature [26, 27], we are able to fit the experimental spectrum. This happens through optimization of the biomolecules concentrations (oxyhaemoglobin, deoxyhaemoglobin, water, fat, bile), and scattering amplitude α, Mie scattering power β, and Rayleigh scattering ratio γ, i.e, the contribution of Rayleigh scattering to the total scattering (equations 2 and 3). Considering these three types of inputs, our first initial guess is made for seven or eight parameters to be optimised, depending on the investigated tissue. The algorithm then accesses the respective reflectance value from our LUT model.

Calculation of optical properties uses the following equations:

$$\mu_{a\ total}(\lambda) = \Sigma\, f_{chromophore}\, \mu_{a,chromophore}(\lambda) \quad (2)$$

$$\mu_{s\ total} = \alpha \left[(1-\gamma)\left(\frac{\lambda}{\lambda_0}\right)^{-\beta} + \gamma \left(\frac{\lambda}{\lambda_0}\right)^{-4}\right] \quad (3),$$

where $f_{Chromophore}$ and $\mu_{a,Chromophore}$ are the volume percent of each chromophore and its absorption coefficient in the pure state, respectively. Our model considers oxyhaemoglobin (HbO_2), deoxyhemoglobin (Hb), water, fat, and bile as chromophores in liver, while only the first four were taken into account for heart and kidney. In this study, we will refer to $f_{blood} = f_{Hb} + f_{HbO_2}$ as blood volume percentage (BVP).

After this, an optimization of the biomolecules concentrations and scattering amplitudes (α and γ) and power (β) takes place by using the trust-region-reflective algorithm of the nonlinear least-squares solver implemented in MATLAB (Mathworks, Nattick, Massachusetts). The process is repeated until the difference between the experimental and

calculated reflectance reaches a threshold limit, i.e., the optimization stops after the error reaches the tolerance limit of 10^{-7} (figure 2).

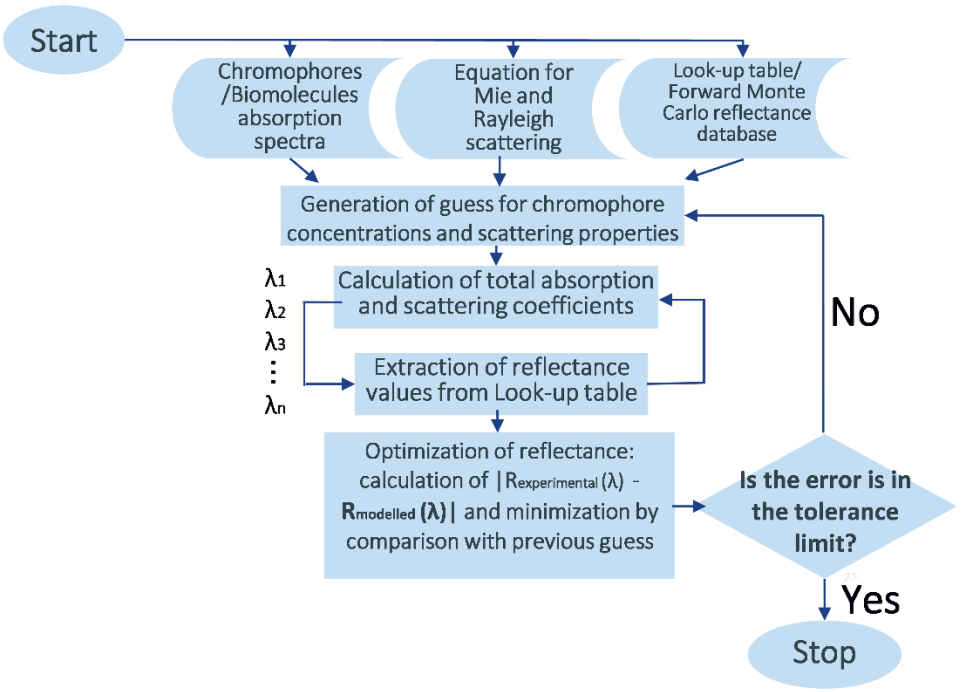

Figure 2: Flowchart of our spectral fitting algorithm.

Once μ_s is determined, the calculation of the reduced scattering coefficient μ_s' is given by:

$$\mu'_{s\ total} = \mu_{s\ total}\ (1 - g) \tag{4}$$

$$\mu'_{s\ total} = \alpha' \left[(1-\gamma)\left(\frac{\lambda}{\lambda_0}\right)^{-\beta} + \gamma\left(\frac{\lambda}{\lambda_0}\right)^{-4}\right] \tag{5},$$

where g is the anisotropy factor, assumed to be equal to 0.9, and $\alpha' = \alpha(1-g)$ is the scattering amplitude for μ_s' values.

In addition to scattering parameters and volume percent of each chromophore, we calculated the total haemoglobin concentration (THC) by using the equation reported by Jacques, S. L. [155], assuming the mass concentration within blood as 150 g L^{-1} and molecular weight of average haemoglobin as 64 458 g mol^{-1}.

3. RESULTS AND DISCUSSION

3.1 Reproducibility analysis for different temperature and pressure states

The reproducibility of the shape of the spectrum was evaluated for the cortex of each organ. This reproducibility involve aspects of both tissue morphology and biochemistry. Morphological information include organization of multicellular structures (such as vessels, fibres, nerves), cells size, number of organelles, composition of tissue layers, extracellular matrix, membranes, and other factors that may contribute for the heterogeneity of tissue refractive index.

Most of these factors are associated to scattering properties. On the other hand, biochemical features such as water, blood, lipid, bile, bilirubin, melanin, collagen content are primarily related to absorption properties. All these characteristics can affect reflectance measurements depending on the tissue type and methodological conditions in which each study is carried out. Difference in average reflectance spectra of heart, kidney and liver is shown in figure 3. By observing kidney spectra, lower blood content is clearly seen by the decreased absorption between 525 and 575 nm.

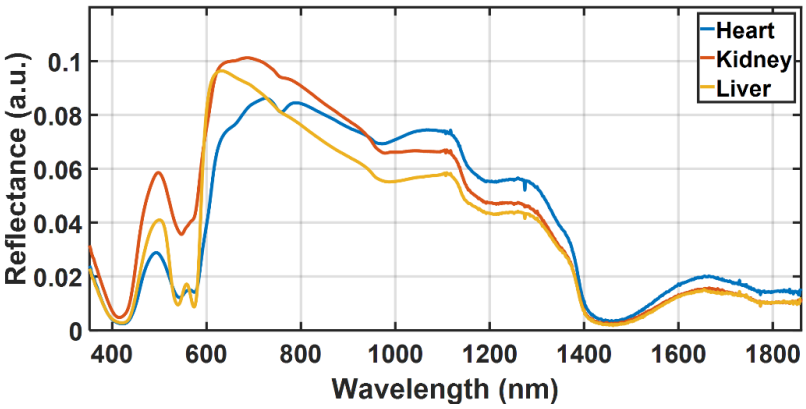

Figure 3: Average diffuse reflectance spectra for 25 °C in heart, kidney and liver when the surface of the fibre optic probe is touching the organ.

One way to investigate the temperature effect in tissue diffuse reflectance measurements is monitoring changes in its optical properties. These properties were mostly studied for temperatures above 20°C. In this case, current literature covers research about μ_s' changes due to dehydration of collagen fibres, transition of glycolipids of cell membranes from a gel to a liquid phase, protein denaturation or degradation of cellular components.

Troy et al. described temperature effects in optical properties of several types of tissues for optical mammography (infiltrating carcinoma, ductal carcinoma in situ, mucinous carcinoma, normal fatty, and normal fibrous tissues) [149]. They observed a variation in the absorption coefficient (between 0.25 and 0.7 cm^{-1}) and reduced scattering coefficient (between 0 and 30 cm^{-1}) of canine prostate tissue upon temperature increase from 23 to 64 °C. They attributed the increase in the scattering coefficient to the degradation of cellular components, although this increase happened even for temperatures below the tissue coagulation threshold (around 60 °C) [156]. In addition, they reported no significant difference was detected in tissue optical properties at 633 nm after repeatedly freezing and thawing samples in room temperature [149].

Laufer et al. studied the effect of temperatures between 20 to 45 °C in optical properties of human *ex vivo* skin. These properties are studied in a spectral range of 600 to 1050 nm. In both dermis and subdermis, no significant change in the absorption coefficient (μ_a) was observed. On the other hand, the reduced scattering coefficient (μ_s') increased as a function of temperature for the dermal tissue, whereas it decreased for the subdermis. Changes in subdermis are explained by a transition from a gel phase (stable crystalline phase) of glycolipids in human cell membranes to a liquid-crystalline phase when increasing the temperature from 25 to 45 °C. Conversely, variations of μ_s' in dermis were assumed to originate from changes in hydration of its collagen fibre structure.

Jaywant et al also reported a μ_s' increase (at wavelengths 633 nm and 810 nm) in bovine muscle and liver tissues at temperatures between 40 and 80 °C [153]. They correlated this increase in muscle to denaturation of actin (loss of sarcomere I band up to 45 °C) and myosin (denaturation of sarcomere A band up to 70 °C). In liver, μ_s' changes were attributed to denaturation of a set of globulin proteins in a variety of temperatures.

Our data shows a more intense diffuse reflectance signal at lower temperatures for heart and kidney tissues (figure 4). Since there was a little difference in the spectra shape, we believe the reasons for this increase are mainly related to tissue scattering properties. Heart has several layers including pericardial adipose tissue, fibrous pericardium, pericardial cavity with serous pericardial fluid, epicardium (with mesothelial cells and connective tissue), myocardium (containing cardiac muscle), and endocardium. Since mice heart is small we might be able to interrogate most of these tissues. Then,

possible reasons for the measurement of a stronger reflectance intensity (figure 4A) may include a transition of lipids in adipose tissue and glycolipids in cell membranes to a more "crystalline" phase in 0 °C, hydration of collagen fibres in connective tissue, and changes in actin-myosin complexes due to muscle contraction. Kidney tissue layers include an adipose tissue layer, renal capsule (layer of connective tissue containing collagen and elastin), renal fascia (mostly composed by connective tissue), cortex (highly vascularized and granular tissue with nephrons, composed by renal corpuscles and tubules), medulla (containing a dense nephron network), and renal pelvis. Due to a similar organization of tissue layers (outer adipose and connective tissues), possible reasons for the increase in the measured diffuse reflectance (figure 4B) may be similar what we listed for heart tissue, except by alterations in actin-myosin complexes. Liver has several lobes separated by ligaments (collagen-rich connective tissue). Their surface is covered by a network of collagen and elastin fibers that make up the Glisson's capsule. Right below this capsule, liver parenchyma is mainly composed by hepatocytes, Kupffer cells, stellate cells and endothelial cells. Liver is a highly perfused organ with hepatocytes lining small vessels (sinusoids) and participating in the metabolism of several components such as lipids, proteins and bile. This means liver parenchyma absorption is dominated by blood and bile as long as there is no fat accumulation (such as in steatosis cases). Since a decrease in the liver reflectance was observed at 0 °C and the shape of the spectrum changed, an increase in the local chromophore concentration and haemoglobin oxygenation may explain this alteration. Since the intensity in the haemoglobin and water absorption regions remain stable, the intensity decrease in other spectral regions may be mostly caused by changes in bile concentration and blood oxygenation. In addition, variations in scattering properties may interfere with the detected reflectance intensity.

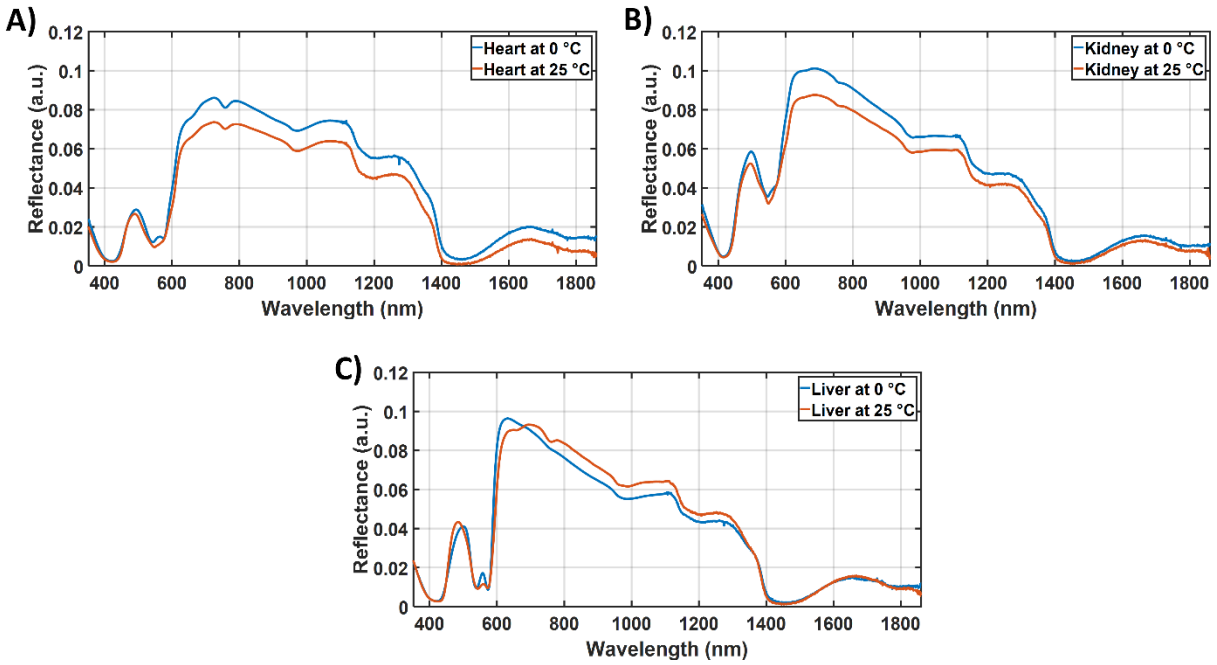

Figure 4: Average diffuse reflectance spectra for 0 °C and 25 °C in A) heart, B) kidney, and C) liver. A more intense diffuse reflectance was obtained at lower temperatures for heart and kidney tissues.

As described previously for temperature effects in the diffuse reflectance signal, pressure influence can also be studied by measuring changes in tissue optical properties. Reported analyses support effects of increased local blood volume when raising the probe pressure against tissue, possible increase of water concentration due to compression of intracellular fluids, and increase of refractive index heterogeneity. Ti et al. investigated effects of probe contact pressure in the diffuse reflectance signals (wavelengths between 400 nm and 900 nm) of heart and liver tissues. After elevating this pressure, they observed major alterations between 400 and 650 nm. These alterations were attributed to a decreased in local blood volume in the measurement region due to a typical tissue response under focal pressure. They concluded the hemodynamics of local tissue should be taken into account when collecting diffuse reflectance spectra [143]. Although this statement agreed with the results showed by Chan, et al. [142], this latter research group reported that

tissue compression could lead to an increase in the absorption coefficient. In the visible wavelength range, this was explained by an increase of local chromophore concentration upon reduction of tissue thickness. For the infrared region, it was justified by the retainment of intracellular fluids during compression, which increases the volumetric water concentration. Difference between these studies (Ti et al. [143] and Chan, et al. [142]) may happen because they use a different settings for tissue geometry (semi-infinite medium and slab configurations) and status (*in vivo* and *ex vivo*). They also described an increase of μ_s' and suggested structural changes generated by this compression increase the effective scatterer concentration. This happened because tissue density and refractive index become more heterogeneous when its thickness is reduced. The μ_s' increase was also reported by Reif et al., who analysed reflectance spectra fitting parameters in mice thigh muscle [138].

With this in mind, we believe the diffuse reflectance of heart tissue increases upon compression (figure 5 A) because the density of refractive index mismatches become higher. In addition, the stability of the near-infrared range above 1380 nm may imply an increase in the local water volume. In regards to kidney tissue, no significant changes are observed after increasing the fibre contact pressure. This suggests most of the reflectance intensity is not influenced by the outer adipose tissue layer at 25 °C.

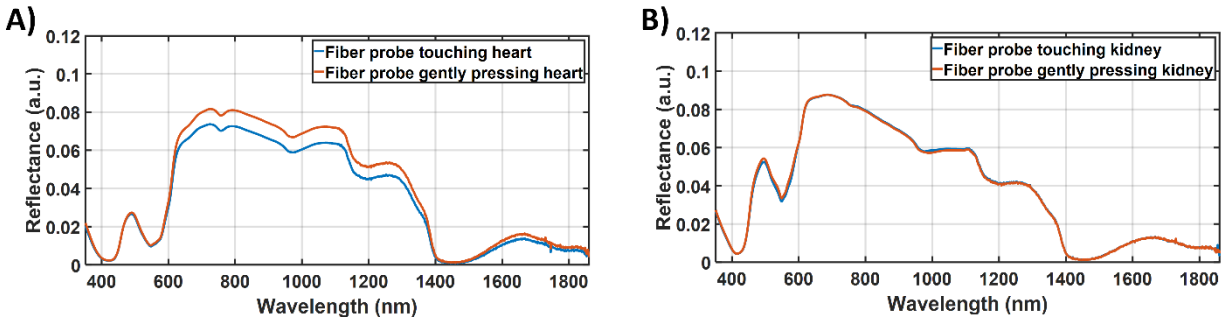

Figure 5: Average diffuse reflectance spectra for two measurement conditions in A) heart and B) kidney: when the surface of the fiber optic probe is touching the interrogated area or when this probe is gently pressing the organ surface at 25 °C.

In regards to the reproducibility of the shape of reflectance measurements, both internal and external reproducibility are mostly higher at 25 °C (tables 1 and 2). Also, both reproducibility values increase with temperature and applied pressure for heart tissue. On the other hand, kidney values are lower for greater pressures at 0 °C. When comparing values of internal and external reproducibility, i.e., extending the comparison of measurements in the same organ to measurements in all organs, an increase was obtained for heart at 0 °C, whereas a slight decrease is observed in kidney (except by the condition of 0 °C and applied contact pressure. Overall, liver provided the most homogeneous shape of the reflectance spectrum.

Table 1: Internal reproducibility of reflectance measurements for each organ type. The shape of heart spectra is more heterogeneous than kidney and liver.

Organ		**Probe contact pressure**	
		Touch	**Gently pressing**
	Temperature		
Heart (n = 2)	**0 °C**	0.855198 ± 0.00003	0.87 ± 0.10
	25 °C	0.91 ± 0.05	0.96 ± 0.01
Kidney (n = 3)	**0 °C**	0.97 ± 0.02	0.88 ± 0.05
	25 °C	0.92 ± 0.01	0.94 ± 0.01
Liver (n = 3)	**0 °C**	0.94 ± 0.01	-
	25 °C	0.96 ± 0.02	-

Table 2: External reproducibility of reflectance measurements for each organ type. The shape of heart spectra is more heterogeneous than kidney and liver.

Organ		Probe contact pressure	
		Touch	Gently pressing
	Temperature		
Heart (n = 2)	**0 °C**	0.88	0.89
	25 °C	0.9	0.96
Kidney (n = 3)	**0 °C**	0.96	0.9
	25 °C	0.91	0.93
Liver (n = 3)	**0 °C**	0.93	-
	25 °C	0.96	-

Since heart had a relatively low but recurrent internal irreproducibility (0 °C and fibre touch the tissue surface) and an improved external reproducibility when extending the comparison for measurements among organs, it shows the highest variability in one of its conditions (table 3). When comparing values of organ variability, liver exhibits most stable measurements, while kidney shows a relatively high variability at 25 °C. For kidney, the measurement condition of touching the tissue surface leads to a lower influence of organ structure and composition in the diffuse reflectance. This should be taken into account for future studies involving different temperatures in renal tissue.

Table 3: Variability of reflectance measurements in each organ type and measurement condition. Liver has the lowest biological variability in 25 °C, whereas kidney presents the most stable reflectance at 0 °C. Even though error in internal and external reproducibility was rounded off to one significant figure in tables 1 and 2, we considered the full values of average and standard deviation to calculate variability values.

Organ		Probe contact pressure	
		Touch	Gently pressing
	Temperature		
Heart (n = 2)	**0 °C**	908.2	0.2
	25 °C	0.2	0.2
Kidney (n = 3)	**0 °C**	0.3	0.2
	25 °C	0.5	0.9
Liver (n = 3)	**0 °C**	0.3	-
	25 °C	0.1	-

Compared to the previous external reproducibility values, an improvement of measurements reproducibility was obtained for average of reflectance spectra in each type of organ (table 4). A great improvement was achieved particularly for conditions where external reproducibility was equal or below 0.91 (table 2). This suggests the average reflectance of at least 3 measurements in different regions is stable among organs, especially during their assessment in cold temperatures. This assessment includes organ viability for transplantation after cold preservation through simple static cold storage or hypothermic machine perfusion.

Table 4: External reproducibility of average of reflectance measurements in each organ type. An improvement can be observed compared to values calculated for single measurements.

Organ		Probe contact pressure	
		Touch	Gently pressing
	Temperature		
Heart (n = 2)	**0 °C**	0.98	0.99
	25 °C	0.94	0.98
Kidney (n = 3)	**0 °C**	0.98	0.97
	25 °C	0.96	0.97
Liver (n = 3)	**0 °C**	0.98	-
	25 °C	0.99	-

3.2 Extraction of tissue optical properties and chromophore concentrations

In this section, we present variations of parameters obtained in our spectral fitting in the same measurement conditions specified in the last section. These parameters are also compared with those reported in previous studies in order to evaluate the accuracy of our analysis and investigate additional implementations to improve our fitting algorithm (figure 6). Our error percentage, calculated by the difference between the experimental and fitted spectra divided by the experimental reflectance for each wavelength, is especially low in the spectral range from 600 nm to 1300 nm. Accuracy improvements will be achieved by expanding our chromophore database and changing the geometry of our fibre optic probe. This will allow us to obtain more precise values of both tissue optical properties (figure 7) and chromophore concentrations.

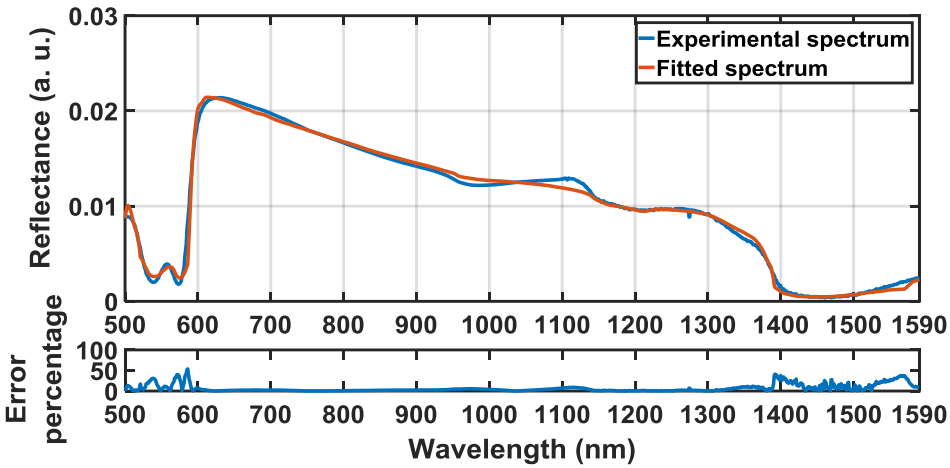

Figure 6: Comparison between an example of experimental spectrum and the inverse Monte Carlo spectral fitting. We are improving the accuracy of the fitting by measuring improved chromophore spectra in an extended wavelength range. Error percentage is calculated by the difference between the experimental and fitted spectra divided by the experimental reflectance for each wavelength.

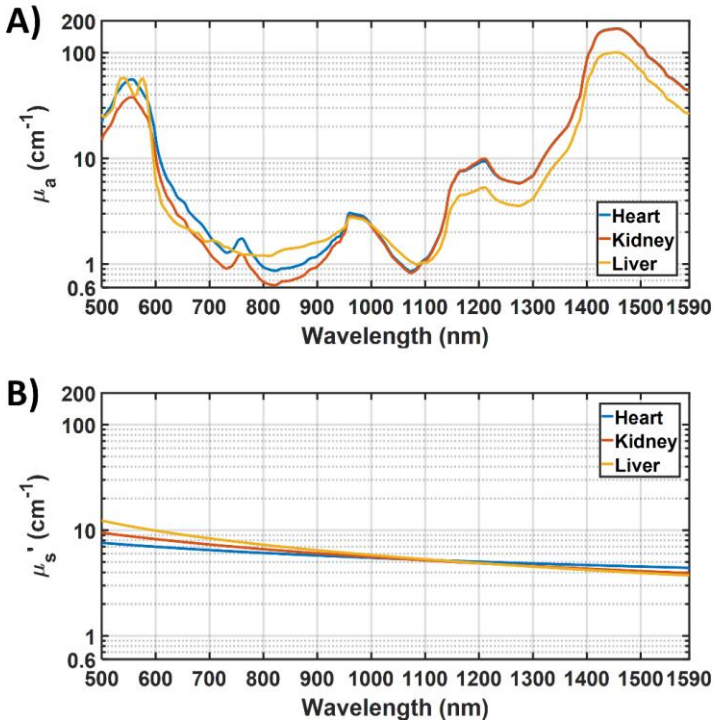

Figure 7: A) Absorption coefficient and B) reduced scattering coefficient for a typical spectrum of heart, kidney and liver obtained in this study. Features of blood and water absorption can be observed in spectral ranges from 500 to 800 nm and above 1100 nm, respectively.

We observed very different features in both μ_a and μ_s' spectra. μ_a values typically varied from 0.6 to 200 cm^{-1}, while μ_s' was restricted between 2 and 20 cm^{-1} (figure 7). As mentioned for diffuse reflectance spectra, kidney tissue had less influence of blood absorption in the interrogated volume of our measurements. On the other hand, a high blood content is observed in heart (table 5), especially when increasing the probe contact pressure in the tissue surface. This also happens for the scattering amplitude. This amplitude is lower for measurements in 25 °C, whereas the Rayleigh scattering ratio is lower for 0 °C. Signals captured at 0 °C with the probe touching in the tissue surface tend to have lower BVP and THC.

Some studies report values for optical properties and chromophore concentration in heart and muscle tissues. Scepanovic et al. studied the diffuse reflectance of excised human carotid endarterectomy specimens with intraplaque haemorrhage in a spectral region between 300 nm and 700 nm. They report a total Hb concentration of 0 to 16 mg/mL (0 to 248.2 µM) and scattering amplitude between 1 and 4 cm^{-1} [25]. This scattering amplitude agrees with the value reported by Nachabé et al (2010). They measured muscle diffuse reflectance in a spectral range between 500 nm and 1600 nm using a fibre optic probe with 2.48 mm of source-to-detector distance. Their spectral fitting parameters included scattering amplitude of 4.6 cm^{-1}, Mie scattering power of 0.6, Mie-to-Rayleigh scattering fraction of 87%, and BVP of 2% [27]. Our study shows higher values for all these parameters, particularly BVP and scattering amplitude (table 5). This may happen because we conducted experiments in *ex vivo* tissues, which may have differences with measurements performed in *in vivo* tissues by their research group. In addition, we measured layers of different tissue types with a different probe geometry so that the interrogated volume may include a different volume of muscle tissue compared to their study. However, our values of total haemoglobin concentration (THC) agree with part of the values reported by Scepanovic et al. In addition, the scattering power and Mie-to-Rayleigh scattering fraction are close to what Nachabé et al described**.**

In regards to effects of probe contact pressure in heart tissue, our study agrees with what is reported by Reif et al., who analysed reflectance spectra fitting parameters in mice thigh muscle [138]. They used the spectral region from 350 to 700 nm to study effects of compression in the blood volume fraction, oxygen saturation, blood vessel radius, Mie slope, and reduced scattering coefficient. No trend was observed in the mean blood volume fraction (variation up to 20%), whereas μ_s' increased with applied pressure. Conversely, a decrease in oxygen saturation, blood vessel radius, and

Mie slope (Mie scattering power) was described. When comparing our measurements for heart tissue at 25 °C, the same trend in the mean BVP, Mie scattering power, and μ_s' is observed.

Table 5: Spectral fitting parameters for heart tissue in each measurement condition. A decrease in BVP and THC is observed when touching the fibre optic probe in the organ surface at 0 °C. At this temperature, the Rayleigh scattering ratio decreases significantly, whereas the scattering amplitude is lower for 25 °C. Also, we perceived a higher BVP, THC and scattering amplitude when gently pressing the fibre optic probe in the heart surface.

	Touch		**Gently pressing**	
Spectral fitting parameters (Heart)	**0 °C**	**25 °C**	**0 °C**	**25 °C**
Blood volume %	10.29	11.96	12.25	12.68
Total Hb concentration (µM)	239	278	285	295
Scattering amplitude α' (cm^{-1})	7.9	7.0	8.6	7.7
Mie scattering power β	0.41	0.4	0.46	0.37
Rayleigh scattering ratio γ (%)	10^{-9}	10^{-6}	$2*10^{-9}$	10^{-6}

Kidney tissue has a decrease in all spectral fitting parameters, except by the Rayleigh scattering ratio, for measurements taken at in higher temperatures or upon application of probe contact pressure (table 6). Reduction in the scattering parameters at 25 °C may be related to phase transition of lipids in adipose tissue, whereas the decrease with applied pressure may be associated with water displacement from collagen fibrils in connective tissue, which creates a more refractive index-matched environment, as described by Chan et. al. [142]. Lower blood content might be explained by the local exsanguination upon compression investigated by Ti et al.

Studies presenting values of chromophore concentrations in kidney include two reported assessments of blood content and oxygenation during induced renal ischemia by Grosenick et al. [23] and Goel et. al [24]. Grosenick et al. obtained a THC of 580 µM and scattering power of around 2 for renal tissue before aortic occlusion. This was done by using time-resolved near-infrared spectroscopy in the wavelengths 690 nm, 800 nm and 830 nm. After occlusion, THC drops to around 450 µM and scatter power remains almost constant. They also report μ_s' values of 13 cm^{-1} (690 nm), 10 cm^{-1} (800 nm), 9 cm^{-1} (830 nm), and μ_a of 1.35 cm^{-1} (690 nm), 1.14 cm^{-1} (800 nm), 1.18 cm^{-1} (830 nm) before occlusion [23]. Another paper using a similar system increases the number of animals for better sample statistics. It informs the mean of these values as 12.2 cm^{-1} (690 nm), 10.2 cm^{-1} (800 nm), 9.7 cm^{-1} (830 nm) for μ_s', and 0.71 cm^{-1} (690 nm), 0.64 cm^{-1} (800 nm), 0.69 cm^{-1} (830 nm) for μ_a [29]. μ_a values at 800 and 830 nm are very close to what we observed in this study (figure 7), while μ_s' coefficients are comparable. Grosenick et al. also provided a mean THC of 334 µM, which is around 3 times higher than our values (table 6). Even though time-domain near-infrared spectroscopy is considered precise, a study from Goel et. al. showed a difference in both THC and μ_s' in renal tissues. They reported a THC of 10 to 40 µM and and wavelength- averaged μ_s' ranging from 5 to 40 cm^{-1} [24]. These values are closer to what we obtained (table 6). This discrepancy in the values may originate from methodological differences and the optical technique used to extract them.

Table 6: Spectral fitting parameters for kidney tissue in each measurement condition. Decrease can be noticed in all parameters, except by the Rayleigh scattering ratio, were obtained at higher temperatures (25 °C) or upon application of probe contact pressure.

	Touch		**Gently pressing**	
Spectral fitting parameters (Kidney)	**0 °C**	**25 °C**	**0 °C**	**25 °C**
Blood volume %	4.9	4.56	4.37	4.16
Total Hb concentration (µM)	114	106	102	96
Scattering amplitude α' (cm^{-1})	9.3	8.0	9.2	7.9
Mie scattering power β	0.79	0.7	0.75	0.69
Rayleigh scattering ratio γ (%)	$4*10^{-9}$	$3*10^{-8}$	$6*10^{-8}$	$6*10^{-8}$

Liver tissue presented a decrease in BVP, THC and Mie scattering power at higher temperature (25 °C), while bile volume percentage, scattering amplitude and Rayleigh scattering ratio increase. Liver optical properties and chromophores concentrations have been recently investigated in experiments with a semi-infinite medium geometry instead of a tissue slab one. Some of these studies include research from Nachabé et al (2011) [26], Evers et al [28], and Wang et al [31]. By using the same system as for their study in muscle tissue, Nachabé et al (2011) compared chromophore parameters in normal liver and metastatic tumours using reflectance measurements between 500 nm and 1600 nm. The median and standard deviation for these parameters were bile percentage of (5.5±2.3)%, blood volume fraction (or BVP) of (3.2±1.6)%, Mie-to-total scattering fraction of (44±25)%, Mie scattering power/slope of (1.2±0.7), and μ_s' (800 nm) of (17±3) cm^{-1} [26]. A later study (2013) from the same research group includes data of more patients. It showed values of THC varying from 0 to 250 µM (median 79 µM), Bile percentage from 0 to 30% (median 6%), Scattering amplitude from 10 to 40 cm^{-1} (median 19 cm^{-1}, and Mie to total scattering ratio from 0 to 100% (median 35%) [28]. These latter two parameters are close to what we obtained (Mie scattering ratio = 100% - Rayleigh scattering ratio = 66%, table 7) at 25 °C. Our Mie scattering power is also comparable to what they obtained in their first study (table 7). On the other hand, the median of THC and bile percentage are around 3 and 15 times lower than what we determined, respectively.

In regards to liver tissue optical properties, a study from Wang et al. used the diffusion equation to investigate reflectance spectra of human intraperitoneal tissues between 600 nm and 800 nm. They informed values of μ_s' and μ_a (630 nm) are, respectively, 27.53 and 1.46 before photodynamic therapy, 28.76 and 1.42 after it [31], although they were unable to extract oxygenation and THC from liver tissues. Our μ_s' are around 3 times lower, but μ_a values agree with their study (figure 7).

Table 7: Spectral fitting parameters for liver tissue in each measurement condition. An increase of BVP and THC is observed when touching the fibre optic probe in the organ surface at 0 °C. At this temperature, the Rayleigh scattering ratio decreases significantly, whereas the scattering amplitude is higher for 25 °C.

	Temperature	
Spectral fitting parameters (Liver)	**0 °C**	**25 °C**
Blood volume %	12.49	11.15
Total Hb concentration (µM)	291	259
Bile volume %	30	94
Scattering amplitude α' (cm^{-1})	9.3	11.1
Mie scattering power β	0.94	0.61
Rayleigh scattering ratio γ (%)	8	34

Overall, we obtained the lowest value of BVP and THC for kidney tissue, whereas lowest Mie scattering power was noticed for heart. Liver exhibited the highest scattering amplitude at 25 °C, and a high variation of all parameters but this amplitude when comparing data from 0 and 25 °C. The same occur for heart when considering the first two parameters.

4. CONCLUSIONS

This paper presents an evaluation of the reproducibility of diffuse reflectance spectra and biological parameters based on tissue optical properties in different measurement conditions. This evaluation was performed through analysis of heart, kidney and liver tissues at two different temperatures (0 °C and 25 °C) and contact pressure conditions (touching the sample or gently pressing it). We showed an increased stability of diffuse reflectance measurements at 25 °C compared to 0 °C. A good reproducibility in the shape of reflectance spectra was achieved for both kidney and liver in the measurement conditions described in this study. On the other hand, heart tissue reflectance is stable only at 25 °C. However, a higher reproducibility for this organ was obtained when comparing averaged measurements. We also report absorption, scattering properties, and biological parameters comparable to other studies. Lowest blood volume percentage and THC were observed in kidney tissue, whereas lowest Mie scattering power was noticed for heart. In addition, highest scattering amplitude was found in liver at 25 °C. In this organ, a high variation was obtained for blood volume percentage, THC and Mie scattering power for different temperatures. The same occur for heart when

considering the first two parameters. Overall, our results illustrate expected fluctuations in extracted optical-properties-based parameters from diffuse reflectance spectra of highly perfused organs. These organs are more susceptible to drug effects during their administration, thus leading to possible functional impairments. Therefore, DRS can be used to monitor organ functionality in real-time and our study reports predicted parameters for the analysis of this functionality. Moreover, our study gives an insight about assessment of organs viability for transplantation in cases of cold preservation (using methods such as simple static cold storage or hypothermic machine perfusion). This could be done with our estimation of chromophore concentrations and scattering properties, which provide biochemical and morphological information about the investigated tissues. In order to use DRS for diagnostics and surgical guidance, our spectral fitting and its parameters will be improved by introducing new chromophore data in a broader wavelength range in order to increase the accuracy of our inverse MC LUT model. We will also use a new fiber optic probe with longer source-to-detector distance. This will increase the influence of chromophores absorption in our captured signal so that we may be able to obtain more precise biochemical information.

AUTHOR CONTRIBUTIONS STATEMENT

M.S.N. designed the study, assembled, calibrated, and characterized the DRS system, performed the forward MC simulations, generated the MC look-up table, helped to develop the spectral fitting algorithm, implemented the algorithm for data processing, collected, post-processed, analysed, and interpreted the data, participated in discussions regarding topics presented in this study, wrote and revised the paper. M.R. implemented the spectral fitting algorithm, performed the convolution for the light source, participated in discussions regarding this algorithm, and revised the paper. J.G. participated in discussions regarding the spectral fitting algorithm, implemented the algorithm to integrate the photon fluence in the detector area. K.G. provided access to the mouse organs. K.K. helped to improve the MATLAB script for data processing. H.L. is helping to measure chromophore spectra (data not shown) to be used as an input for the spectral fitting algorithm. S.A.E. helped to develop the spectral fitting algorithm, supervised the study, revised the paper, and participated in all discussions related to topics presented in this study.

REFERENCES

[1] A. N. Bashkatov, E. A. Genina, V. I. Kochubey *et al.*, "Optical properties of human stomach mucosa in the spectral range from 400 to 2000nm: Prognosis for gastroenterology," Medical Laser Application, 22(2), 95-104 (2007).

[2] X. Huang, and M. A. El-Sayed, "Gold nanoparticles: Optical properties and implementations in cancer diagnosis and photothermal therapy," Journal of Advanced Research, 1(1), 13-28 (2010).

[3] B. Khlebtsov, V. Zharov, A. Melnikov *et al.*, "Optical amplification of photothermal therapy with gold nanoparticles and nanoclusters," Nanotechnology, 17(20), 5167-5179 (2006).

[4] J. T. Robinson, S. M. Tabakman, Y. Liang *et al.*, "Ultrasmall reduced graphene oxide with high near-infrared absorbance for photothermal therapy," J Am Chem Soc, 133(17), 6825-31 (2011).

[5] A. P. Castano, T. N. Demidova, and M. R. Hamblin, "Mechanisms in photodynamic therapy: part one—photosensitizers, photochemistry and cellular localization," Photodiagnosis and Photodynamic Therapy, 1(4), 279-293 (2004).

[6] N. Honda, K. Ishii, T. Terada *et al.*, "Determination of the tumor tissue optical properties during and after photodynamic therapy using inverse Monte Carlo method and double integrating sphere between 350 and 1000 nm," J Biomed Opt, 16(5), 058003 (2011).

[7] T. C. Zhu, J. C. Finlay, and S. M. Hahn, "Determination of the distribution of light, optical properties, drug concentration, and tissue oxygenation in-vivo in human prostate during motexafin lutetium-mediated photodynamic therapy," J Photochem Photobiol B, 79(3), 231-41 (2005).

[8] X. Huang, I. H. El-Sayed, W. Qian *et al.*, "Cancer cell imaging and photothermal therapy in the near-infrared region by using gold nanorods," J Am Chem Soc, 128(6), 2115-20 (2006).

[9] T. J. Farrell, M. S. Patterson, and B. Wilson, "A diffusion theory model of spatially resolved, steady-state diffuse reflectance for the noninvasive determination of tissue optical properties in vivo," Med Phys, 19(4), 879-88 (1992).

[10] A. Maier, U. Anegg, B. Fell *et al.*, "Effect of photodynamic therapy in a multimodal approach for advanced carcinoma of the gastro-esophageal junction," Lasers in Surgery and Medicine, 26(5), 461-466 (2000).

[11] L. Tong, Q. Wei, A. Wei *et al.*, "Gold nanorods as contrast agents for biological imaging: optical properties, surface conjugation and photothermal effects," Photochem Photobiol, 85(1), 21-32 (2009).
[12] L. Brancaleon, and H. Moseley, "Laser and non-laser light sources for photodynamic therapy," Lasers Med Sci, 17(3), 173-86 (2002).
[13] A. M. Nilsson, R. Berg, and S. Andersson-Engels, "Measurements of the optical properties of tissue in conjunction with photodynamic therapy," Appl Opt, 34(21), 4609-19 (1995).
[14] C. J. Hourdakis, and A. Perris, "A Monte Carlo estimation of tissue optical properties for use in laser dosimetry," Physics in Medicine and Biology, 40(3), 351-364 (1995).
[15] J. V. E. Roche, C. Whitehurst, P. Watt *et al.*, "Photodynamic Therapy (PDT) of Gastrointestinal Tumours: A New Light Delivery System," Lasers in Medical Science, 13(2), 137-142 (1998).
[16] B. C. Wilson, and M. S. Patterson, "The physics of photodynamic therapy," Physics in Medicine and Biology, 31(4), 327-360 (1986).
[17] M. S. Patterson, B. Chance, and B. C. Wilson, "Time resolved reflectance and transmittance for the non-invasive measurement of tissue optical properties," Appl Opt, 28(12), 2331-6 (1989).
[18] M. D. Daniell, and J. S. Hill, "A HISTORY OF PHOTODYNAMIC THERAPY," Australian and New Zealand Journal of Surgery, 61(5), 340-348 (1991).
[19] Q. Chen, B. C. Wilson, S. D. Shetty *et al.*, "Changes in In Vivo Optical Properties and Light Distributions in Normal Canine Prostate during Photodynamic Therapy," Radiation Research, 147(1), 86-91 (1997).
[20] E. M. H. Mathus-Vliegen, and G. N. J. Tytgat, "Nd-YAG laser photocoagulation in gastroenterology: Its role in palliation of colorectal cancer," Lasers in Medical Science, 1(1), 75-80 (1986).
[21] N. Krasner, P. T. Chatlani, and H. Barr, "Photodynamic therapy of tumours in gastroenterology—a review," Lasers in Medical Science, 5(2), 233-239 (1990).
[22] C. H. Sibata, V. C. Colussi, N. L. Oleinick *et al.*, "Photodynamic therapy: a new concept in medical treatment," Brazilian Journal of Medical and Biological Research, 33(8), 869-880 (2000).
[23] B. J. Tromberg, D. Grosenick, O. Steinkellner *et al.*, "Near-infrared spectroscopy of renal tissue in vivo," 8578, 85781P (2013).
[24] U. O. Goel, M. M. Maddox, K. N. Elfer *et al.*, "Feasibility of quantitative diffuse reflectance spectroscopy for targeted measurement of renal ischemia during laparoscopic partial nephrectomy," J Biomed Opt, 19(10), 107001 (2014).
[25] O. R. Scepanovic, M. Fitzmaurice, J. A. Gardecki *et al.*, "Detection of morphological markers of vulnerable atherosclerotic plaque using multimodal spectroscopy," J Biomed Opt, 11(2), 021007 (2006).
[26] R. Nachabe, D. J. Evers, B. H. Hendriks *et al.*, "Effect of bile absorption coefficients on the estimation of liver tissue optical properties and related implications in discriminating healthy and tumorous samples," Biomed Opt Express, 2(3), 600-14 (2011).
[27] R. Nachabe, B. H. Hendriks, M. van der Voort *et al.*, "Estimation of biological chromophores using diffuse optical spectroscopy: benefit of extending the UV-VIS wavelength range to include 1000 to 1600 nm," Biomed Opt Express, 1(5), 1432-1442 (2010).
[28] D. J. Evers, R. Nachabe, D. Hompes *et al.*, "Optical sensing for tumor detection in the liver," Eur J Surg Oncol, 39(1), 68-75 (2013).
[29] T. Niendorf, A. Pohlmann, K. Arakelyan *et al.*, "Detailing renal hemodynamics and oxygenation in rats by a combined near-infrared spectroscopy and invasive probe approach," Acta Physiol (Oxf), 213(1), 19-38 (2015).
[30] J. H. Nilsson, N. Reistad, H. Brange *et al.*, "Diffuse Reflectance Spectroscopy for Surface Measurement of Liver Pathology," Eur Surg Res, 58(1-2), 40-50 (2017).
[31] H. W. Wang, T. C. Zhu, M. E. Putt *et al.*, "Broadband reflectance measurements of light penetration, blood oxygenation, hemoglobin concentration, and drug concentration in human intraperitoneal tissues before and after photodynamic therapy," J Biomed Opt, 10(1), 14004 (2005).
[32] T. M. Breslin, "Autofluorescence and Diffuse Reflectance Properties of Malignant and Benign Breast Tissues," Annals of Surgical Oncology, 11(1), 65-70 (2003).
[33] G. M. Palmer, C. Zhu, T. M. Breslin *et al.*, "Comparison of multiexcitation fluorescence and diffuse reflectance spectroscopy for the diagnosis of breast cancer (March 2003)," IEEE Trans Biomed Eng, 50(11), 1233-42 (2003).
[34] E. Edell, S. Lam, H. Pass *et al.*, "Detection and localization of intraepithelial neoplasia and invasive carcinoma using fluorescence-reflectance bronchoscopy: an international, multicenter clinical trial," J Thorac Oncol, 4(1), 49-54 (2009).
[35] E. Drakaki, E. Kaselouris, M. Makropoulou *et al.*, "Laser-induced fluorescence and reflectance spectroscopy for the discrimination of basal cell carcinoma from the surrounding normal skin tissue," Skin Pharmacol Physiol, 22(3), 158-65 (2009).

[36] J. A. Freeberg, J. L. Benedet, C. MacAulay *et al.*, "The performance of fluorescence and reflectance spectroscopy for the in vivo diagnosis of cervical neoplasia; point probe versus multispectral approaches," Gynecol Oncol, 107(1 Suppl 1), S248-55 (2007).
[37] P. A. Valdes, F. Leblond, V. L. Jacobs *et al.*, "Quantitative, spectrally-resolved intraoperative fluorescence imaging," Sci Rep, 2, 798 (2012).
[38] I. Georgakoudi, E. E. Sheets, M. G. Müller *et al.*, "Trimodal spectroscopy for the detection and characterization of cervical precancers in vivo," American Journal of Obstetrics and Gynecology, 186(3), 374-382 (2002).
[39] I. J. Bigio, and J. R. Mourant, "Ultraviolet and visible spectroscopies for tissue diagnostics: fluorescence spectroscopy and elastic-scattering spectroscopy," Physics in Medicine and Biology, 42(5), 803-814 (1997).
[40] J. Q. Brown, K. Vishwanath, G. M. Palmer *et al.*, "Advances in quantitative UV-visible spectroscopy for clinical and pre-clinical application in cancer," Curr Opin Biotechnol, 20(1), 119-31 (2009).
[41] D. Y. Churmakov, I. V. Meglinski, S. A. Piletsky *et al.*, "Analysis of skin tissues spatial fluorescence distribution by the Monte Carlo simulation," Journal of Physics D: Applied Physics, 36(14), 1722-1728 (2003).
[42] R. M. P. Doornbos, R. Lang, M. C. Aalders *et al.*, "The determination ofin vivohuman tissue optical properties and absolute chromophore concentrations using spatially resolved steady-state diffuse reflectance spectroscopy," Physics in Medicine and Biology, 44(4), 967-981 (1999).
[43] T. Papaioannou, N. W. Preyer, Q. Fang *et al.*, "Effects of fiber-optic probe design and probe-to-target distance on diffuse reflectance measurements of turbid media: an experimental and computational study at 337 nm," Applied Optics, 43(14), 2846 (2004).
[44] R. A. Sheth, R. Upadhyay, L. Stangenberg *et al.*, "Improved detection of ovarian cancer metastases by intraoperative quantitative fluorescence protease imaging in a pre-clinical model," Gynecol Oncol, 112(3), 616-22 (2009).
[45] J. Frangioni, "In vivo near-infrared fluorescence imaging," Current Opinion in Chemical Biology, 7(5), 626-634 (2003).
[46] J. W. Tunnell, A. E. Desjardins, L. Galindo *et al.*, "Instrumentation for multi-modal spectroscopic diagnosis of epithelial dysplasia," Technol Cancer Res Treat, 2(6), 505-14 (2003).
[47] I. Pavlova, K. Sokolov, R. Drezek *et al.*, "Microanatomical and Biochemical Origins of Normal and Precancerous Cervical Autofluorescence Using Laser-scanning Fluorescence Confocal Microscopy¶," Photochemistry and Photobiology, 77(5), 550 (2003).
[48] H.-U. Gremlich, V. Martínez, R. Kneuer *et al.*, "Noninvasive Assessment of Gastric Emptying by Near-Infrared Fluorescence Reflectance Imaging in Mice: Pharmacological Validation with Tegaserod, Cisapride, and Clonidine," Molecular Imaging, 3(4), 153535002004041 (2004).
[49] H.-U. Gremlich, V. Martínez, R. Kneuer *et al.*, "Noninvasive Assessment of Gastric Emptying by Near-Infrared Fluorescence Reflectance Imaging in Mice: Pharmacological Validation with Tegaserod, Cisapride, and Clonidine," Molecular Imaging, 3(4), 15353500200404127 (2004).
[50] A. Liebert, H. Wabnitz, H. Obrig *et al.*, "Non-invasive detection of fluorescence from exogenous chromophores in the adult human brain," Neuroimage, 31(2), 600-8 (2006).
[51] N. Thekkek, and R. Richards-Kortum, "Optical imaging for cervical cancer detection: solutions for a continuing global problem," Nat Rev Cancer, 8(9), 725-31 (2008).
[52] W. J. Cottrell, A. R. Oseroff, and T. H. Foster, "Portable instrument that integrates irradiation with fluorescence and reflectance spectroscopies during clinical photodynamic therapy of cutaneous disease," Review of Scientific Instruments, 77(6), 064302 (2006).
[53] K. R. Diamond, M. S. Patterson, and T. J. Farrell, "Quantification of fluorophore concentration in tissue-simulating media by fluorescence measurements with a single optical fiber," Applied Optics, 42(13), 2436 (2003).
[54] P. A. Valdes, F. Leblond, A. Kim *et al.*, "Quantitative fluorescence in intracranial tumor: implications for ALA-induced PpIX as an intraoperative biomarker," J Neurosurg, 115(1), 11-7 (2011).
[55] K. Vishwanath, B. Pogue, and M.-A. Mycek, "Quantitative fluorescence lifetime spectroscopy in turbid media: comparison of theoretical, experimental and computational methods," Physics in Medicine and Biology, 47(18), 3387-3405 (2002).
[56] P. A. Valdes, V. Jacobs, B. T. Harris *et al.*, "Quantitative fluorescence using 5-aminolevulinic acid-induced protoporphyrin IX biomarker as a surgical adjunct in low-grade glioma surgery," J Neurosurg, 123(3), 771-80 (2015).
[57] C.-C. Yu, C. Lau, G. O'Donoghue *et al.*, "Quantitative spectroscopic imaging for non-invasive early cancer detection," Optics Express, 16(20), 16227 (2008).
[58] K. O. Vasquez, C. Casavant, and J. D. Peterson, "Quantitative whole body biodistribution of fluorescent-labeled agents by non-invasive tomographic imaging," PLoS One, 6(6), e20594 (2011).
[59] J. M. Coremans, C. Ince, H. A. Bruining *et al.*, "(Semi-)quantitative analysis of reduced nicotinamide adenine dinucleotide fluorescence images of blood-perfused rat heart," Biophysical Journal, 72(4), 1849-1860 (1997).

[60] C. Du, A. P. Koretsky, I. Izrailtyan *et al.*, "Simultaneous detection of blood volume, oxygenation, and intracellular calcium changes during cerebral ischemia and reperfusion in vivo using diffuse reflectance and fluorescence," J Cereb Blood Flow Metab, 25(8), 1078-92 (2005).
[61] P. A. Valdes, F. Leblond, A. Kim *et al.*, "A spectrally constrained dual-band normalization technique for protoporphyrin IX quantification in fluorescence-guided surgery," Opt Lett, 37(11), 1817-9 (2012).
[62] F. C. Delori, "Spectrophotometer for noninvasive measurement of intrinsic fluorescence and reflectance of the ocular fundus," Appl Opt, 33(31), 7439-52 (1994).
[63] I. Pavlova, M. Williams, A. El-Naggar *et al.*, "Understanding the biological basis of autofluorescence imaging for oral cancer detection: high-resolution fluorescence microscopy in viable tissue," Clin Cancer Res, 14(8), 2396-404 (2008).
[64] D. Stasic, T. J. Farrell, and M. S. Patterson, "The use of spatially resolved fluorescence and reflectance to determine interface depth in layered fluorophore distributions," Physics in Medicine and Biology, 48(21), 3459-3474 (2003).
[65] T. Hasan, D. H. Kessel, C. Kurachi *et al.*, "Subcellular localization and photodynamic activity of Photodithazine (glucosamine salt of chlorin e6) in murine melanoma B16-F10: an in vitro and in vivo study," Proc SPIE, 44 (2018).
[66] A. Cosci, M. S. Nogueira, S. Prataviera *et al.*, "Erratum: Time-resolved fluorescence spectroscopy for clinical diagnosis of actinic cheilitis: erratum," Biomed Opt Express, 9(2), 648 (2018).
[67] L. Carvalho, M. S. Nogueira, L. P. M. Neto *et al.*, "Erratum: Raman spectral post-processing for oral tissue discrimination - a step for an automatized diagnostic system: erratum," Biomed Opt Express, 9(2), 649 (2018).
[68] L. Carvalho, M. S. Nogueira, L. P. M. Neto *et al.*, "Raman spectral post-processing for oral tissue discrimination - a step for an automatized diagnostic system," Biomed Opt Express, 8(11), 5218-5227 (2017).
[69] C. de Paula Campos, C. de Paula D'Almeida, M. S. Nogueira *et al.*, "Fluorescence spectroscopy in the visible range for the assessment of UVB radiation effects in hairless mice skin," Photodiagnosis Photodyn Ther, 20, 21-27 (2017).
[70] A. Cosci, M. S. Nogueira, S. Prataviera *et al.*, "Time-resolved fluorescence spectroscopy for clinical diagnosis of actinic cheilitis," Biomed Opt Express, 7(10), 4210-4219 (2016).
[71] M. Saito Nogueira, and C. Kurachi, "Assessing the photoaging process at sun exposed and non-exposed skin using fluorescence lifetime spectroscopy," Proc SPIE, 9703, 97031W (2016).
[72] M. Saito Nogueira, A. Cosci, S. Prataviera *et al.*, "Evaluation of actinic cheilitis using fluorescence lifetime spectroscopy," Proc SPIE, 9703, 97031U (2016).
[73] D. H. Kessel, T. Hasan, C. Teles de Andrade *et al.*, "Optical spectroscopy of radiotherapy and photodynamic therapy responses in normal rat skin shows vascular breakdown products," Proc SPIE, 9694, 969410 (2016).
[74] C. d. P. D´Almeida, C. Campos, M. Saito Nogueira *et al.*, "Time-resolved and steady-state fluorescence spectroscopy for the assessment of skin photoaging process," Proc SPIE, 9531, 953146 (2015).
[75] A. P. da Silva, M. Saito Nogueira, J. A. Jo *et al.*, "Optical Based Diagnosis and Treatment of Onychomycosis," Proc SPIE, JTu3A.37 (2016).
[76] C. Kurachi, K. Svanberg, B. J. Tromberg *et al.*, "Assembly and characterization of a fluorescence lifetime spectroscopy system for skin lesions diagnostic," Proc SPIE, 9531, 95313D (2015).
[77] L. Pires, M. S. Nogueira, S. Prataviera *et al.*, "Time-resolved fluorescence lifetime for cutaneous melanoma detection," Biomed Opt Express, 5(9), 3080-9 (2014).
[78] C. Kurachi, L. Pires, M. S. Nogueira *et al.*, "Lifetime fluorescence for the detection of skin lesions," BS4B.3 (2014).
[79] M. S. Nogueira, A. Cosci, R. G. T. Rosa *et al.*, "Portable fluorescence lifetime spectroscopy system for in-situ interrogation of biological tissues." 22, 10.
[80] A. Pifferi, J. Swartling, E. Chikoidze *et al.*, "Spectroscopic time-resolved diffuse reflectance and transmittance measurements of the female breast at different interfiber distances," Journal of Biomedical Optics, 9(6), 1143-1151 (2004).
[81] M. S. Patterson, B. Chance, and B. C. Wilson, "Time resolved reflectance and transmittance for the non-invasive measurement of tissue optical properties," Appl Opt, 28, 2331-2336 (1989).
[82] B. C. Wilson, and S. L. Jacques, "Optical reflectance and transmittance of tissues: principles and applications," IEEE.J.Quant.Electron., 26(12), 2186-2199 (1990).
[83] A. Pifferi, P. Taroni, G. Valentini *et al.*, "Real-time method for fitting time-resolved reflectance and transmittance measurements with a monte carlo model," Appl Opt, 37(13), 2774-80 (1998).
[84] A. Pifferi, J. Swartling, E. Chikoidze *et al.*, "Spectroscopic time-resolved diffuse reflectance and transmittance measurements of the female breast at different interfiber distances," J Biomed Opt, 9(6), 1143-51 (2004).
[85] T. Svensson, R. Savo, E. Alerstam *et al.*, "Exploiting breakdown of the similarity relation for diffuse light transport: simultaneous retrieval of scattering anisotropy and diffusion constant," Optics Letters, 38(4), 437-439 (2013).
[86] A. Pifferi, P. Taroni, G. Valentini *et al.*, "Real-time method for fitting time-resolved reflectance and transmittance measurements with a Monte Carlo model," Applied Optics, 37(13), 2774-2780 (1998).

[87] R. Graaff, A. C. Dassel, M. H. Koelink *et al.*, “Optical properties of human dermis in vitro and in vivo,” Appl Opt, 32(4), 435-47 (1993).
[88] A. Pifferi, P. Taroni, G. Valentini *et al.*, “Real-time method for fitting time-resolved reflectance and transmittance measurements with a Monte Carlo model,” Applied Optics, 37(13), 2774 (1998).
[89] T. M. Bydlon, R. Nachabe, N. Ramanujam *et al.*, “Chromophore based analyses of steady-state diffuse reflectance spectroscopy: current status and perspectives for clinical adoption,” J Biophotonics, 8(1-2), 9-24 (2015).
[90] M. D. Keller, S. K. Majumder, M. C. Kelley *et al.*, “Autofluorescence and diffuse reflectance spectroscopy and spectral imaging for breast surgical margin analysis,” Lasers Surg Med, 42(1), 15-23 (2010).
[91] A. M. Laughney, V. Krishnaswamy, P. B. García-Allende *et al.*, "Automated classification of breast pathology using local measures of broadband reflectance." 15, 12.
[92] V. P. Wallace, J. C. Bamber, D. C. Crawford *et al.*, “Classification of reflectance spectra from pigmented skin lesions, a comparison of multivariate discriminant analysis and artificial neural networks,” Physics in Medicine and Biology, 45(10), 2859-2871 (2000).
[93] S. K. Majumder, M. D. Keller, F. I. Boulos *et al.*, "Comparison of autofluorescence, diffuse reflectance, and Raman spectroscopy for breast tissue discrimination." 13, 11.
[94] C. Zhu, G. M. Palmer, T. M. Breslin *et al.*, “Diagnosis of breast cancer using diffuse reflectance spectroscopy: Comparison of a Monte Carlo versus partial least squares analysis based feature extraction technique,” Lasers Surg Med, 38(7), 714-24 (2006).
[95] C. Zhu, G. M. Palmer, T. M. Breslin *et al.*, "Diagnosis of breast cancer using fluorescence and diffuse reflectance spectroscopy: a Monte-Carlo-model-based approach." 13, 15.
[96] J. L. Jayanthi, G. U. Nisha, S. Manju *et al.*, “Diffuse reflectance spectroscopy: diagnostic accuracy of a non-invasive screening technique for early detection of malignant changes in the oral cavity,” BMJ Open, 1(1), e000071 (2011).
[97] M. B. Wallace, L. T. Perelman, V. Backman *et al.*, “Endoscopic detection of dysplasia in patients with Barrett's esophagus using light-scattering spectroscopy,” Gastroenterology, 119(3), 677-682 (2000).
[98] R. J. Nordstrom, L. Burke, J. M. Niloff *et al.*, “Identification of cervical intraepithelial neoplasia (CIN) using UV-excited fluorescence and diffuse-reflectance tissue spectroscopy,” Lasers Surg Med, 29(2), 118-27 (2001).
[99] K. Maruo, M. Tsurugi, M. Tamura *et al.*, “In Vivo Noninvasive Measurement of Blood Glucose by Near-Infrared Diffuse-Reflectance Spectroscopy,” Applied Spectroscopy, 57(10), 1236-1244 (2003).
[100] G. O. Angheloiu, J. T. Arendt, M. G. Muller *et al.*, “Intrinsic fluorescence and diffuse reflectance spectroscopy identify superficial foam cells in coronary plaques prone to erosion,” Arterioscler Thromb Vasc Biol, 26(7), 1594-600 (2006).
[101] C. E. R. Weber, R. A. Schwarz, E. N. Atkinson *et al.*, "Model-based analysis of reflectance and fluorescence spectra for in vivo detection of cervical dysplasia and cancer." 13, 10.
[102] S. Fantini, S. A. Walker, M. A. Franceschini *et al.*, “Assessment of the size, position, and optical properties of breast tumors in vivo by noninvasive optical methods,” Applied Optics, 37(10), 1982 (1998).
[103] T. Durduran, R. Choe, J. P. Culver *et al.*, “Bulk optical properties of healthy female breast tissue,” Physics in Medicine and Biology, 47(16), 2847-2861 (2002).
[104] A. H. Hielscher, R. E. Alcouffe, and R. L. Barbour, “Comparison of finite-difference transport and diffusion calculations for photon migration in homogeneous and heterogeneous tissues,” Physics in Medicine and Biology, 43(5), 1285-1302 (1998).
[105] V. Ntziachristos, and R. Weissleder, “Experimental three-dimensional fluorescence reconstruction of diffuse media by use of a normalized Born approximation,” Optics Letters, 26(12), 893 (2001).
[106] H. Jiang, “Frequency-domain fluorescent diffusion tomography: a finite-element-based algorithm and simulations,” Applied Optics, 37(22), 5337 (1998).
[107] B. W. Pogue, and M. S. Patterson, “Frequency-domain optical absorption spectroscopy of finite tissue volumes using diffusion theory,” Physics in Medicine and Biology, 39(7), 1157-1180 (1994).
[108] J. B. Fishkin, O. Coquoz, E. R. Anderson *et al.*, “Frequency-domain photon migration measurements of normal and malignant tissue optical properties in a human subject,” Applied Optics, 36(1), 10 (1997).
[109] T. A. Erickson, A. Mazhar, D. J. Cuccia *et al.*, "Lookup-table method for imaging optical properties with structured illumination beyond the diffusion theory regime." 15, 9.
[110] B. J. Tromberg, O. Coquoz, J. B. Fishkin *et al.*, “Non–invasive measurements of breast tissue optical properties using frequency–domain photon migration,” Philosophical Transactions of the Royal Society of London. Series B: Biological Sciences, 352(1354), 661-668 (1997).
[111] D. Contini, F. Martelli, and G. Zaccanti, “Photon migration through a turbid slab described by a model based on diffusion approximation I Theory,” Applied Optics, 36(19), 4587 (1997).
[112] B. J. Tromberg, L. O. Svaasand, T. T. Tsay *et al.*, “Properties of photon density waves in multiple-scattering media,” Appl Opt, 32(4), 607-16 (1993).

[113] D. J. Cuccia, F. P. Bevilacqua, A. J. Durkin *et al.*, "Quantitation and mapping of tissue optical properties using modulated imaging." 14, 13.
[114] L. V. Wang, and S. L. Jacques, "Source of error in calculation of optical diffuse reflectance from turbid media using diffusion theory," Computer Methods and Programs in Biomedicine, 61(3), 163-170 (2000).
[115] K. D. Paulsen, and H. Jiang, "Spatially varying optical property reconstruction using a finite element diffusion equation approximation," Med Phys, 22(6), 691-701 (1995).
[116] D. Arifler, C. E. MacAulay, M. Follen *et al.*, "Spatially resolved reflectance spectroscopy for diagnosis of cervical precancer: Monte Carlo modeling and comparison to clinical measurements." 11, 16.
[117] Z. Shi, and C. A. Anderson, "Application of Monte Carlo simulation-based photon migration for enhanced understanding of near-infrared (NIR) diffuse reflectance. Part I: Depth of penetration in pharmaceutical materials," J Pharm Sci, 99(5), 2399-412 (2010).
[118] C. Zhu, and Q. Liu, "Review of Monte Carlo modeling of light transport in tissues," J Biomed Opt, 18(5), 50902 (2013).
[119] M. Sharma, R. Hennessy, M. K. Markey *et al.*, "Verification of a two-layer inverse Monte Carlo absorption model using multiple source-detector separation diffuse reflectance spectroscopy," Biomed Opt Express, 5(1), 40-53 (2013).
[120] E. Péry, W. C. P. M. Blondel, C. Thomas *et al.*, "Diffuse Reflectance Spectroscopy Monte-Carlo Modeling: Elongated Arterial Tissues Optical Properties," IFAC Proceedings Volumes, 39(18), 41-46 (2006).
[121] F. Bevilacqua, and C. Depeursinge, "Monte Carlo study of diffuse reflectance at source–detector separations close to one transport mean free path," Journal of the Optical Society of America A, 16(12), 2935 (1999).
[122] G. Yao, and L. V. Wang, "Monte Carlo simulation of an optical coherence tomography signal in homogeneous turbid media," Physics in Medicine and Biology, 44(9), 2307-2320 (1999).
[123] S. J. Madsen, B. C. Wilson, M. S. Patterson *et al.*, "Experimental tests of a simple diffusion model for the estimation of scattering and absorption coefficients of turbid media from time-resolved diffuse reflectance measurements," Appl Opt, 31(18), 3509-17 (1992).
[124] A. Doronin, and I. Meglinski, "Online object oriented Monte Carlo computational tool for the needs of biomedical optics," Biomed Opt Express, 2(9), 2461-9 (2011).
[125] Q. Liu, and N. Ramanujam, "Scaling method for fast Monte Carlo simulation of diffuse reflectance spectra from multilayered turbid media," Journal of the Optical Society of America A, 24(4), 1011 (2007).
[126] M. Hiraoka, M. Firbank, M. Essenpreis *et al.*, "A Monte Carlo investigation of optical pathlength in inhomogeneous tissue and its application to near-infrared spectroscopy," Physics in Medicine and Biology, 38(12), 1859-1876 (1993).
[127] G. Zonios, and A. Dimou, "Modeling diffuse reflectance from homogeneous semi-infinite turbid media for biological tissue applications: a Monte Carlo study," Biomed Opt Express, 2(12), 3284-94 (2011).
[128] H. Arimoto, M. Egawa, and Y. Yamada, "Depth profile of diffuse reflectance near-infrared spectroscopy for measurement of water content in skin," Skin Res Technol, 11(1), 27-35 (2005).
[129] C. M. Gardner, S. L. Jacques, and A. J. Welch, "Light transport in tissue: Accurate expressions for one-dimensional fluence rate and escape function based upon Monte Carlo simulation," Lasers in Surgery and Medicine, 18(2), 129-138 (1996).
[130] B. C. Wilson, and G. Adam, "A Monte Carlo model for the absorption and flux distributions of light in tissue," Med Phys, 10(6), 824-30 (1983).
[131] S. T. Flock, B. C. Wilson, and M. S. Patterson, "Monte Carlo modeling of light propagation in highly scattering tissues--II: Comparison with measurements in phantoms," IEEE Trans Biomed Eng, 36(12), 1169-73 (1989).
[132] J. C. Finlay, and T. H. Foster, "Hemoglobin oxygen saturations in phantoms and in vivo from measurements of steady-state diffuse reflectance at a single, short source-detector separation," Med Phys, 31(7), 1949-59 (2004).
[133] N. Reistad, J. Nilsson, O. Vilhelmsson Timmermand *et al.*, "Diffuse reflectance spectroscopy of liver tissue." 9531, 95314E-95314E-10 (2015).
[134] I. Fredriksson, M. Larsson, and T. Stromberg, "Inverse Monte Carlo method in a multilayered tissue model for diffuse reflectance spectroscopy," J Biomed Opt, 17(4), 047004 (2012).
[135] N. Rajaram, T. H. Nguyen, and J. W. Tunnell, "Lookup table-based inverse model for determining optical properties of turbid media," J Biomed Opt, 13(5), 050501 (2008).
[136] R. Hennessy, S. L. Lim, M. K. Markey *et al.*, "Monte Carlo lookup table-based inverse model for extracting optical properties from tissue-simulating phantoms using diffuse reflectance spectroscopy," J Biomed Opt, 18(3), 037003 (2013).
[137] X. Zhong, X. Wen, and D. Zhu, "Lookup-table-based inverse model for human skin reflectance spectroscopy: two-layered Monte Carlo simulations and experiments," Opt Express, 22(2), 1852-64 (2014).
[138] R. Reif, M. S. Amorosino, K. W. Calabro *et al.*, "Analysis of changes in reflectance measurements on biological tissues subjected to different probe pressures," J Biomed Opt, 13(1), 010502 (2008).

[139] N. Reistad, M. Mayjonade, A. Ahadi *et al.*, "Characterization of probe contact effects on diffuse reflectance spectroscopy measurements." 9531, 953143.
[140] R. L. P. van Veen, H. j. c. m. Sterenborg, A. Pifferi *et al.*, "Determination of VIS- NIR absorption coefficients of mammalian fat, with time- and spatially resolved diffuse reflectance and transmission spectroscopy," SF4 (2004).
[141] J. Laufer, R. Simpson, M. Kohl *et al.*, "Effect of temperature on the optical properties ofex vivohuman dermis and subdermis," Physics in Medicine and Biology, 43(9), 2479-2489 (1998).
[142] E. K. Chan, B. Sorg, D. Protsenko *et al.*, "Effects of compression on soft tissue optical properties," IEEE Journal of Selected Topics in Quantum Electronics, 2(4), 943-950 (1996).
[143] Y. Ti, and W.-C. Lin, "Effects of probe contact pressure on in vivo optical spectroscopy," Optics Express, 16(6), 4250 (2008).
[144] E. Salomatina, and A. N. Yaroslavsky, "Evaluation of the in vivo and ex vivo optical properties in a mouse ear model," Phys Med Biol, 53(11), 2797-807 (2008).
[145] M. Mesradi, A. Genoux, V. Cuplov *et al.*, "Experimental and analytical comparative study of optical coefficient of fresh and frozen rat tissues," J Biomed Opt, 18(11), 117010 (2013).
[146] J. S. Dam, C. B. Pedersen, T. Dalgaard *et al.*, "Fiber-optic probe for noninvasive real-time determination of tissue optical properties at multiple wavelengths," Applied Optics, 40(7), 1155 (2001).
[147] R. Sfareni, A. Boffi, V. Quaresima *et al.*, "Near infrared absorption spectra of human deoxy- and oxyhaemoglobin in the temperature range 20–40°C," Biochimica et Biophysica Acta (BBA) - Protein Structure and Molecular Enzymology, 1340(2), 165-169 (1997).
[148] T. L. Troy, and S. N. Thennadil, "Optical properties of human skin in the near infrared wavelength range of 1000 to 2200 nm," J Biomed Opt, 6(2), 167-76 (2001).
[149] T. L. Troy, D. L. Page, and E. M. Sevick-Muraca, "Optical properties of normal and diseased breast tissues: prognosis for optical mammography," J Biomed Opt, 1(3), 342-55 (1996).
[150] R. N. A. H. Lewis, D. A. Mannock, R. N. McElhaney *et al.*, "Physical properties of glycosyldiacylglycerols: an infrared spectroscopic study of the gel-phase polymorphism of 1,2-di-O-acyl-3-O-(.beta.-D-glucopyranosyl)-sn-glycerols," Biochemistry, 29(38), 8933-8943 (2002).
[151] S. L. Jacques, H. Shangguan, S. A. Prahl *et al.*, "Pressure effects on soft tissues monitored by changes in tissue optical properties," 3254, 366 (1998).
[152] A. Kienle, L. Lilge, M. S. Patterson *et al.*, "Spatially resolved absolute diffuse reflectance measurements for noninvasive determination of the optical scattering and absorption coefficients of biological tissue," Appl Opt, 35(13), 2304-14 (1996).
[153] S. L. Jacques, S. M. Jaywant, A. Katzir *et al.*, "Temperature-dependent changes in the optical absorption and scattering spectra of tissues: correlation with ultrastructure," 1882, 218 (1993).
[154] B. M. Q. Weaver, G. E. Staddon, and M. R. B. Pearson, "Tissue blood content in anaesthetised sheep and horses," Comparative Biochemistry and Physiology Part A: Physiology, 94(3), 401-404 (1989).
[155] S. L. Jacques, "Corrigendum: Optical properties of biological tissues: a review," Physics in Medicine and Biology, 58(14), 5007-5008 (2013).
[156] J. S. Suri, [Advances in diagnostic and therapeutic ultrasound imaging] Artech House, (2008).